Micro-structural Investigations on Oppositely Charged Mixed Surfactant Gels With Potential Dermal Applications

Manas Barai
Vidyasagar University
Emili Manna
Vidyasagar University
Habiba Sultana
Vidyasagar University
Manas Mandal
Vidyasagar University
Kartik Guchhait
Vidyasagar University
Tuhin Manna
Vidyasagar University
Anuttam Patra
Luleå University of Technology
Chien-Hsiang Chang
National Cheng Kung University
Parikshit Moitra
Indian Association for the Cultivation of Science
Chandradipa Ghosh
Vidyasagar University
Anna-Carin Larsson
Luleå University of Technology
Santanu Bhattacharya
Indian Association for the Cultivation of Science
Amiya Panda (akpanda@mail.vidyasagar.ac.in)
Department of Chemistry, Vidyasagar University, Midnapore - 721102, West Bengal, India

Research Article

Keywords: Dicarboxylic amino acid-based surfactants, hexadecyltrimethylammonium bromide (HTAB), Staphylococcus aureus

Posted Date: January 22nd, 2021

DOI: https://doi.org/10.21203/rs.3.rs-146590/v1

Version of Record: A version of this preprint was published at Scientific Reports on July 30th, 2021. See the published version at https://doi.org/10.1038/s41598-021-94777-2.

Abstract

Dicarboxylic amino acid-based surfactants (*N*-dodecyl derivatives of -aminomalonate, -aspartate, and -glutamate) in combination with hexadecyltrimethylammonium bromide (HTAB) form a variety of aggregates. Composition and concentration dependent mixtures may exhibit liquid crystal, gel, precipitate and clear isotropic phases. Liquid crystalline patterns were identified by polarization optical microscopy and fluorescence microscopy. FE-SEM studies reveal porous and flower like morphology. Phase transitions and weight loss depend on composition where thermotropic behaviors were revealed through differential scanning calorimetry and thermogravimetric analyses, respectively. Systems comprising more than 60% HTAB demonstrate shear-thinning behavior. Gels cause insignificant toxicity to human peripheral lymphocytes and irritation to mouse skin; they do not display the symptoms of cutaneous irritation, neutrophilic invasion and inflammation (erythema, edema, and skin thinning). Gels also exhibit antibacterial effect on *Staphylococcus aureus*, a potent causative agent of skin and soft tissue infections, suggesting its possible application as vehicle for dermatological drug delivery.

Introduction

Formation of gels and different liquid crystalline phases by oppositely charged mixed surfactant systems depend on composition, surfactant chain length, salinity, temperature, pH and external field, *etc*.[1-5] Artificial gels possess regulated super structure where the properties of the fabricated liquid crystals [6-10] depend on electrostatic, hydrophobic, hydrogen bond, and van der Waals interactions among the components.[11-13] Gels are associated with two independent transitions, *viz.,* sol-gel transition of the gelator and isotropic-anisotropic transition of liquid crystals.[9, 10, 14-18] Rod shaped mesogens exhibit nematic and smectic phase while disk shaped mesogens show columnar phase.[14, 16] Gelatinous property of surfactant aggregates largely depends on the molecular architecture of the aggregating species that control its structure and shape.[14, 19, 20]

Gels have versatile applications in tissue engineering,[21] hemostasis bandages,[22-26] photo patterning,[17, 27-30] 3D-printing,[31, 32] electrochemistry,[33] pharmaceutical formulation[5, 34-36] and regenerative medicine,[10, 37-39] *etc*. Recent advances in the design and synthesis of dicarboxylic Amino Acid based Surfactants (AAS) have opened up its wide range of applications as chelator in metal extraction.[40] Due to its “green nature” the present research groups have studied its aggregation behavior with HTAB where some mixed surfactant formed gel.[16] This has instigated to undertake further investigations on such aggregates at higher concentration with the aim in using them as novel dermatological drug delivery systems.

The main aim of the present work is to undertake physicochemical investigations on different types of aggregates formed by AAS+HTAB. While HTAB shows antimicrobial activities, however, AASs are biocompatible. Because of its toxicity, individual use of HTAB is unwarranted. However, when HTAB is used in combination with AASs, its toxicity is expected to get substantially reduced. To check the biocompatibility of gels and its possible dermatological application, cytotoxicity, skin irritation and

histological studies were carried out. Besides antibacterial activity on *Staphylococcus aureus*, causative factor for persistent skin and tissue infections was explored.

Results And Discussion

Structure of $C_{12}MalNa_2$ and HTAB are shown in (Fig. 1a) along with other information. Gibbs ternary phase diagram (Fig. 1b) studies demonstrate the occurrence of gel, viscous, precipitate and clear fluid states. With increasing proportion of HTAB, mixed aggregates form gel where the relative proportion of viscous and gel states increase that follow the order: $C_{12}MalNa_2 > C_{12}AspNa_2 > C_{12}GluNa_2$ (Fig. S1, supplementary section). Hydrophobic interaction between AASs and HTAB is the predominant factor for the formation of different types of aggregates besides the electrostatic attraction.[8] Carboxylate groups of AASs interact with HTAB at 2:1 ratio and form gel state at equimolar region due to the dominance of HTAB molecule.[41] Microstructural investigations on the gelatinous aggregates were further investigated through polarizing opitical microscopy (POM), fluorescence microscopy (FM) and field emission scanning electron microscopic (FE-SEM) studies.

POM studies reveal the occurrence of liquid crystal and associated textures as

shown in (Fig. 1c). Gels exhibit similar textures in the surfactant concentration range of 3 - 5 wt%. With increasing proportion of HTAB, $C_{12}MalNa_2$ gels display nematic, smectic, spherulite, cholesteric, calamitic, and flower like textures (Fig. S2, Table S2).[41-44] The patterns become more complex with enhanced sizes due to the aggregation and associative interaction between AASs and HTAB. Texture size increases with increasing proportion of HTAB, which has higher cross sectional area than the AASs.[45] Features become more prominent with increasing mixed surfactant concentration, common in case of lyotropic liquid crystals [16, 44] (Fig. S2). In case of $C_{12}AspNa_2$ gels for 50, 60 and 80 wt% HTAB, smectic, spherulite, and flower like patterns are observed,[46, 47] while in case of $C_{12}GluNa_2$ discotic and flower like textures are predominant (Fig. S3). Two carboxylate groups get progressively separated by methylene group while moving from $C_{12}MalNa_2$ to $C_{12}AspNa_2$ to $C_{12}GluNa_2$. Accordingly, two carboxylate groups of AASs can electrostatically interact with one HTAB to form six, seven and eight member rings.[45] Smectic textures designate ordered and rigid layer structure whereby $C_{12}MalNa_2$ can closely interact with HTAB to exhibit smectic texture. The nematic texture is characteristic of stacked layer and positional order whereby the discotic texture is due to rigid disk like core.[48, 49] $C_{12}MalNa_2$ gels display more prominent spherulite texture than $C_{12}AspNa_2$ due to the strongly aggregated structure and associative interaction between AAS and HTAB. $C_{12}AspNa_2$ and $C_{12}GluNa_2$ gels exhibit cholesteric texture because formation of sterically favorable seven and eight member rings (Fig. S2a_4 and c_4). Columnar textures have relatively flexible core, exhibited by $C_{12}GluNa_2$ due to weak hydrophobic interaction.

FM studies display fluorescence active liquid texture. Rhodamine-B and fluorescein were used as cationic and anionic dyes for FM studies. Rhodamine-B shows red fluorescence and binds to the anionic rich sites

of gels (Fig. 1d).[50, 51] Carboxylate groups of AASs interact with HTAB molecules where the systems are mostly anionic with lower proportion of HTAB. Fluorescein shows green fluorescence due to its binding with the cation rich sites (Fig.1e). However, when two dyes are mixed; no specific fluorescence is observed due to the mutual quenching between the dye molecules.[52] Fluorescein weakly interacts with the anion rich mixed surfactants, hence fluorescence is not as strong as rhodamine-B. The prominent fluorescence patterns could be correlated with the textures as observed by POM studies, thus considered to be an alternative method.

Microstructures of the aggregates were further investigated by FE-SEM studies, which display interconnected morphologies (Fig. 1f).[27, 52, 53] With increasing proportion of HTAB, $C_{12}MalNa_2$ gels display rolled, wrinkled, cloth, coral, sponge, porous, and flower like morphologies, (Fig. S4, Table S2)[27, 54, 55] which suggest that the pore of the gels can provide pockets for water molecules to be included by surface tension in achieving optimal solvation and swelling, necessary for hydration. $C_{12}MalNa_2$, in combination with HTAB show flower and coral like morphologies (Fig. S5a_2). In case of $C_{12}AspNa_2$, gels with 50, 60 and 80 wt% of HTAB exhibit fiber, wrinkled and spheroid structures. $C_{12}GluNa_2$ prominently exhibits exposed honeycomb, snowball like microsphere and cloth like intertwined textures (Fig. S5).[27, 28, 54-56] $C_{12}AspNa_2$ and $C_{12}GluNa_2$ gels show characteristic honeycomb like morphology (Fig. S5b_3) due to the emergence of micropores at the surface of gels.[57] Clumped and spheroid texture of $C_{12}MalNa_2$ indicate extended sheet like feature and larger bundle fiber network structure. $C_{12}AspNa_2$ and $C_{12}GluNa_2$ gels have fiber network like morphologies that can hold water molecules due to assisted its higher surface tension (Fig S5 a_2 and b_3). Rolled, wrinkled, and sponge like architectures are due to the existence of protrusions and larger channels for which $C_{12}MalNa_2$ exhibit compact bundle fiber network morphology (Fig. S4a_5 and b_4).[55] Snowball and wrinkled morphologies in case of $C_{12}AspNa_2$ and $C_{12}GluNa_2$ indicate the entrapment of water molecules into the gels. Maximum number of HTAB accumulated in gels indicate that HTAB plays fundamental role in demonstrating higher aggregation and formation of porous like morphology, which are in consonance with the phase manifestation, POM and FM studies.

Phase transition and associated weight loss of gels were investigated with TGA studies.[58-60] Results on the thermogravimetric analysis of the pure components as well as AAS+HTAB aggregates have been summarized in Fig S6 and Table S1 (supplementary section). HTAB decomposes to produce some solid carbon along with the production of long chain hydrocarbon, nitrogen, and hydrogen,[58, 61] whereby decomposition of $C_{12}MalNa_2$, $C_{12}AspNa_2$ and $C_{12}GluNa_2$ to produce dodecane (or smaller alkyl fragments) and -aminomalonic, -aspartic and -glutamic acid.[60] AAS+HTAB gels show endothermic peaks in the temperature range of 40 to 100°C due to the dehydration (Fig 2a).[62]

Two carboxylate groups of $C_{12}MalNa_2$ hydrophobically interact with HTAB that result in higher ionicity and subsequent moisture absorption capability than $C_{12}AspNa_2$ and $C_{12}GluNa_2$. In case of $C_{12}GluNa_2$, two ionic carboxylate groups are separated by three methylene groups; so the interaction capability and

magnitude of hydration is lower. Formation of rigid aggregates result in the higher chain melting temperature (T_m) comparable with the DSC studies.

Thermotropic behavior and associated parameters were evaluated by DSC studies.[41] Variation of phase transition temperature (T_m), width at half peak height ($\Delta T_{1/2}$), enthalpy change (ΔH) and corresponding heat capacity change (ΔC_p) were determined as function of the surfactant composition (mole fraction of AAS, α_{AAS}) as summarized in (Fig. 2). HTAB exhibits two endothermic peaks at 64°C and 84°C due to dehydration,[41] as well as transition from solid to liquid crystalline phase (Fig. 2b), common in the amphiphiles.[60] With increasing α_{AAS}, T_m values increase due to the incorporation of HTAB in the aggregates and assimilation of HTAB with the AASs, relatively sharp peaks appear indicating favorable hydrocarbon chain packing (Fig. 2c).[45] Lowering of T_m is due to size reduction, decreased specific surface area and interaction between oppositely charged surfactants also known as Kelvin effect.[63] T_m values indicate that widening of the peaks designate multi-crystallinity and heterogeneity. The extent of hydrophobic interaction between AAS and HTAB is lower in $C_{12}AspNa_2$ and $C_{12}GluNa_2$, where the T_m values follow the sequence: $C_{12}MalNa_2 > C_{12}AspNa_2 > C_{12}GluNa_2$. With increasing α_{AAS}, $\Delta T_{1/2}$ values decrease indicating better packing of the hydrophilic overlayer as well as oppositely charged head groups (Fig. 2d). With increasing associative interaction between AAS and HTAB increased crystal imperfection results in higher $\Delta T_{1/2}$ values. Increased head group volume, induced through the formation of ion pair amphiphiles, creates energetically unfavorable voids in the hydrocarbon region, resulting higher ΔH values for the surfactant mixtures (Fig. 2e). With increasing α_{AAS}, ΔCp values gradually increase and exhibit endothermicity due to the formation of water overlayer around surfactant aggregates (Fig. 2f). Lower values of ΔCp are due to the increase in multicrystallinity.

Viscosity studies on AAS+HTAB mixtures at different combinations exhibit share thinning.[45] Zero shear viscosity (η_0) *vs.* concentration profile for the gels comprising 60 mole% HTAB are shown in (Fig. 3a).

With increasing surfactant concentration, viscosity increases monotonously in the range of 10 to 100 mM. The sequence in the viscosity variation follow the order $C_{12}MalNa_2 > C_{12}AspNa_2 > C_{12}GluNa_2$, which are in consonance with the previous studies. Due to the stronger packing and subsequent formation of rigid structured aggregates, viscosity of $C_{12}MalNa_2$ system is higher than the other two.

AAS+HTAB aggregates exhibit less toxicity against human blood lymphocyte up to 20 mM; however, it increases with increasing surfactant concentration (Fig. 3b). Cytotoxicities are in consonance with the corresponding viscosity of the mixtures. Gels do not exhibit symptom of cutaneous irritation and inflammation (erythema, edema, skin thinning and neutrophilic invasion) on the dorsal area of the trunk region of mice, similar to the effect of sterile distilled water used as negative control, unlike 5% phenol water (positive control) that causes redness and thinning of skin (Fig. 4a-c).

Histological studies of haematoxylin and eosin stained skins treated with gels, sterile water and 5% phenol were performed to further visualize the presence of any inflammatory response (Fig. 4d-f).[64]

Neutrophil infiltration and aggregation could only be found in phenol treated skins, unlike the gel and water (negative control) treated groups where no neutrophil invasion is observed. Results suggest that the gels can safely be used for topical applications.

Gels also possess substantial activity against gram-positive pathogenic bacteria *Staphylococcus aureus*. In spite of about 90% lymphocyte viability, at 20 mM (AAS:HTAB, 40:60, M/M) the surfactant mixtures are capable to cease bacterial growth (considered to be the minimum inhibitory concentration, MIC value).[65] The gels therefore can potentially be used in the treatment of bacteria born dermatological infections. In addition, the gels are expected to exhibit higher entrapment efficiency and sustained release of dermatological drugs. However, further *in vitro* and *in vivo* studies are warranted to substantiate the potential as drug delivery systems.

Summary And Conclusions

Micro-structures of AAS+HTAB aggregates were investigated by combined phase manifestation, optical and electron microscopic studies. Texture of the liquid crystals formed by the surfactant aggregates depend on its concentration and composition. Energetics of phase transition processes were evaluated by TGA and DSC studies. Cytotoxicity could be correlated with the viscosity of the gels. Gels impart insignificant skin irritation although they possess substantial antibacterial activities that project its potential as dermal drug delivery systems. However further *in vitro* and *in vivo* studies by incorporating appropriate drugs into the gels are necessary and being considered as the future perspectives.

Experimental Section

Materials. Hexadecyltrimethylammonium bromide (HTAB) and histopaque-1077^{TM} were the products from Sigma-Aldrich Chemicals Pvt. Ltd. (USA). Disodium salts of Amino Acid based Surfactants (AAS) were synthesized in our lab following previous published procedure.[66] Phenol, haematoxillin, eosinY and 3-(4,5-dimethylthiazol-2-yl)-2,5-diphenyl tetrazolium bromide (MTT) were purchased from HiMedia Laboratories Pvt. Ltd. India, while Rhodamine-B and fluorescein were obtained from Sisco Research Laboratory Pvt. Ltd. India. Double distilled water was used throughout the experiments. All the chemicals were stated to be ≥ 99% pure.

Methods.

Phase manifestation. Composition, close to the boundary of the two-phase regions, was detected by homogeneous mixing of aqueous stock solution of oppositely charged surfactants at 25°C. The exact boundary of two-phase region was detected further by stepwise addition of higher concentration of AASs into the HTAB solution using a calibrated micropipette under constant stirring. On the basis of visual observation, more than one hundred samples were collected at different AASs and HTAB weight ratio and phase boundaries were identified.[67] The different phases were recorded consecutively for a longer time-

period (at least fifteen days, after which the samples started microbial degradation). All the experiments were repeated thrice to ensure the reproducibility.

Polarization optical microscopy (POM) studies. Texture of different combinations of the mixed surfactant systems were recorded with a polarization optical microscope (Nikon ECLIPSELV100POL, Japan) set with a CCD camera. Sample was placed on to a glass slide and thereafter the POM images were recorded.

Fluorescence microscopic (FM) studies. Mixtures of AASs+HTAB at different combinations were also investigated with fluorescence microscopy doped with three sets of dyes: a) rhodamine B, b) eosin Y, and c) an equimolar mixture of rhodamine-B and eosin Y. Fluorescence images were recorded with an upright microscope (NIKON ECLIPSE LV100POL, Japan) equipped with a green and red fluorescence active CCD camera (model no. DS-Fil).

Field emission scanning electronic microscopy (FE-SEM) studies. Morphology of the surfactant aggregates were investigated with a scanning electron microscope (ZEISS EVO 18, Germany). Samples were prepared by the drop casting the gel on a freshly cleaved mica foil and kept in air for two hours for solvent evaporation. They were further dried at reduced pressure for two hours. The gold sputtered samples were then analyzed for SEM at the operating voltage of20-30 kV.

Thermogravimetric analysis (TGA). The weight loss and thermal stability of the gels were investigated by TGA, performed using Pyris 6 TGA-DTA-8000 (Perkin Elmer, USA). Samples were scanned in the temperature range of 50-500°C with a scan rate of 20°C min^{-1} under nitrogen gas flow.

Differential scanning calorimetric (DSC) studies.DSC studies were performed to evaluate the chain melting temperature (T_m) and associated thermodynamic parameters of mixed surfactant systems thatcontrol its physical states. DSC measurements were recorded using a Pyris 6 DSC-8000 (Perkin Elmer, USA) differential scanning calorimeter with indium as a calibrator before performing the experiment. After equilibrating for 10 min, the sample was scanned in the temperature range 0-273°C with a scan rate of 10°C min^{-1} during the heating cycle, while it was cooled at a scan rate of 5°C min^{-1}. From the thermogram the peak temperature and enthalpy of phase transition were evaluated. Endothermic peak *vs.* temperature in evaluating different physicochemical parameter of mixed surfactant system were considered.[68]

Rheology studies. Viscosity of different surfactant mixtures were determined by a DV II-Pro rotoviscometer (Brookfield, USA) with a stated accuracy of ±0.01 cP. 1.0 mL surfactant solutions of different concentrations(40, 60, 80 and 100 mm) were taken in a cone and plate type rotoviscometer.[69] Viscosities were measured at different shear rate (ranging from 76-380 s^{-1}). Zero shear viscosity (η_0) was determined from the intercept of the plot of viscosity *vs.* shear rate by fitting polynomial regression. Temperature during the viscosity measurements was controlled by a circulatory water bath (Hanntech Corporation, South Korea).

Biological activities.

All the biological experiments were performed in accordance with relevant guidelines and regulations, duly approved by the Institutional Ethic Committee, Vidyasagar University. All the methods were carried out in accordance with relevant guidelines and regulations.

Cytotoxicity studies. Cytotoxicity studies were carried out following the method of Sun.et al.[65] 5 mL of human blood (volunteered by a healthy person) was diluted (1:1) with phosphate buffered saline (PBS) and added to Histopaque-1077. Informed consent was obtained from all subjects. It was centrifuged at 1500 rpm for 40 min at room temperature. The upper monolayer containing lymphocytes was further washed through centrifugation. The lymphocytes were re-suspended in RPMI complete media supplemented with 10% (*w/v*) fetal bovine serum (FBS) and incubated for a day at 37°C in a 5% (*v/v*) CO_2 environment (in CO_2 incubator).[70] Cytotoxicity of selected gels were estimated by MTT assay.[71] 20 µL 5 % (w/v) MTT solutions were added to each well of microtitre plate, having RPMI-suspended lymphocytes with or without the gels. Then the plate was incubated at 37°C for 4 h in metabolizing MTT to formazan. After the aspiration of the supernatant, 100 µL HCl+isopropanoic acid solution (1:1) was added to each well of the culture plate and mixed to dissolve the formazan crystals. The optical density (OD) of the sample was measured on ELISA reader (Model 550, BIO-RAD, USA) using test and reference wavelengths of 570 and 630 nm, respectively. The percentage of cell viability was calculated using the following equation: [71]

$$\text{Cell viability } \% = [OD_{\text{sample}} - OD_{\text{control}}] \text{ X } 100/OD_{\text{control}} \quad (1)$$

Cutaneous irritation test. The cutaneous irritation test was carried out in compliance with the Animal Research: Reporting of *In Vivo* Experiments (ARRIVE) guidelines. Cutaneous irritation test of selected gels were performed as mentioned in the Good Laboratory Practice Standards (GLPS) manual and the guidelines of Organization for Economic Co-operation and Development (OECD) for acute dermal irritation.[65] Thirty healthy Swiss albino mice were divided into five groups, each group consisting six mice. Group A was negative control, treated with sterile distilled water and group B was positive control treated with 5% phenol water to develop skin irritation. Mice of group C, D and E were treated with 100 mM $C_{12}MalNa_2$ + HTAB, $C_{12}AspNa_2$ + HTAB and $C_{12}GluNa_2$ + HTAB gels respectively. Before the test, the hairs of dorsal area of the trunk region of all the mice were removed and each applied topically with 500 µL of respective experimental gels and controls. After 4 h, any sign of erythema or edema in individual animal was recorded. This entire procedure of dermal application of gels and subsequent recording for any irritation was done for consecutive seven days.

Histological studies of mice skin. After seven days of skin irritation study, all the animals were euthanized by carbon dioxide asphyxiation. The treated skins were processed in wax blocks and transverse sections were prepared, followed by staining with hematoxylin-eosinY (HE)[72] and examined under light

microscope (Axioscope A1; Carl Zeiss, Germany). The histology of gel-treated skins was compared with that of the control animals.

Antibacterial activity studies. Antibacterial efficacies of the gels against *Staphylococcus aureus* grown in Luria Bertani (LB) broth were evaluated and minimum inhibitory concentration (MIC) for each gel was determined.[73] MIC is the lowest concentration of the selected component that renders no turbidity in bacterial culture corresponding to 99% of bacterial growth inhibition. To determine MIC of each gel 10 µL bacterial culture having approximately 1×10^7 CFU/mL cells was added to 1 mL of LB. Various diluted samples of the experimental gels were added to the tubes containing the bacterial cells and was incubated overnight. Next day, the MIC value was obtained by testing the turbidity of the bacterial culture.

Declarations

Acknowledgements:

This work has been financially supported by University Grants Commission (UGC), New Delhi, India through a UGC-BSR scheme, (F.25-1/2014-15(BSR)/7-234/2009(BSR) UGC-SAP (No. F. 5-9/ 2015/DRS-II (SAP-II) and Department of Science and Technology, Govt. of India, New Delhi, India through the DST-FIST grants (No. SR/FST/CSI-235/2011 (G) and SR/FST/CS-I/ 2017/7 (C).

Author's Correspondence:

Prof. Amiya Kumar Panda
Department of Chemistry and Chemical Technology

Vidyasagar University

Midnapore-721102

West Bengal, INDIA

Email: akpanda@mail.vidyasagar.ac.in

Phone: +913222298379

Fax: +91322275329/297

Cell:+91 9433347210

Declaration: Authors declare no conflict of interest.

References

1. Fanasca, S., Colla, G., Maiani, G., Venneria, E., Rouphael, Y., Azzini, E., and Saccardo, F. Changes in antioxidant content of tomato fruits in response to cultivar and nutrient solution composition, *J. Agricul. Food Chem.* ***54***, 4319-4325 (2006).
2. Lopez-Leon, T., Fernandez-Nieves, A., Nobili, M., and Blanc, C. Nematic-smectic transition in spherical shells, *Phys. Rev. Let.****106***, 247802 (2011).
3. Pelton, R. Temperature-sensitive aqueous microgels, *Adv. Colloid and Interface Sci.****85***, 1-33 (2000).
4. Saunders, B. R., and Vincent, B. Microgel particles as model colloids: theory, properties and applications, *Adv. Colloid and Interface Sci.****80***, 1-25 (1999).
5. Williams, R. J., Smith, A. M., Collins, R., Hodson, N., Das, A. K., and Ulijn, R. V. Enzyme-assisted self-assembly under thermodynamic control, *Nature Nanotechnol.****4***, 19 (2009).
6. Barker, C. A., Saul, D., Tiddy, G. J. T., Wheeler, B. A., and Willis, E. Phase structure, nuclear magnetic resonance and rheological properties of viscoelastic sodium dodecyl sulphate and trimethylammonium bromide mixtures, *J. Chem. Soc. Far. Trans. 1: Phys. Chem. Cond. Phases****70***, 154-162 (1974).
7. Hammer, S. E., Ebert, M., and Weinbruch, S. Comparison of operator-and computer-controlled scanning electron microscopy of particles from different atmospheric aerosol types, *Anal. Bioanal. Chem.****411***, 1633-1645 (2019).
8. Herrington, K. L., Kaler, E. W., Miller, D. D., Zasadzinski, J. A., and Chiruvolu, S. Phase behavior of aqueous mixtures of dodecyltrimethylammonium bromide (DTAB) and sodium dodecyl sulfate (SDS), *J. Phys. Chem.****97***, 13792-13802 (1993).
9. Jokela, P., Jönsson, B., and Wennerström, H. Phase equilibria in systems containing both an anionic and a cationic amphiphile. A thermodynamic model calculation, *Surf. Ads. surf. Spectro. Disper. Sys.* (Lindman, B., Olofsson, G., and Stenius, P., Eds.), Steinkopff, Darmstadt 17-22, (1985).
10. Sangeetha, N. M., and Maitra, U. (2005) Supramolecular gels: Functions and uses, *Chem. Soc. Rev.* ***34***, 821-836.
11. Ohshima, H., (Ed.) *Catanionic Surfactants: Novel Surrogates of Phospholipids*, John Wiley and Sons, New Jersey, 1, (2016).
12. Holland, P. M., and Rubingh, D. N. Mixed Surfactant Systems, In *Mixed Surfactant Systems*, *Am. Chem. Soc.* 2-30 (1992).
13. Kronberg, B. Surfactant mixtures, *Cur. Opin. Colloid Interface Sci.****2***, 456-463 (1997).
14. Du, X., Zhou, J., Shi, J., and Xu, B. Supramolecular hydrogelators and hydrogels: from soft matter to molecular biomaterials, *Chem. Rev.****115***, 13165-13307 (2015).
15. Hirst, A. R., Escuder, B., Miravet, J. F., and Smith, D. K. High-tech applications of self-assembling supramolecular nanostructured gel-phase materials: from regenerative medicine to electronic devices, *Angew. Chemie****47***, 8002-8018 (2008).
16. Kato, T., Hirai, Y., Nakaso, S., and Moriyama, M. Liquid-crystalline physical gels, *Chem. Soc. Rev.****36***, 1857-1867 (2007).

17. Matsumoto, S., Yamaguchi, S., Ueno, S., Komatsu, H., Ikeda, M., Ishizuka, K., Iko, Y., Tabata, K. V., Aoki, H., and Ito, S. Photo gel–sol/sol–gel transition and its patterning of a supramolecular hydrogel as stimulited responsive biomaterials, *Chem. Eu. J.**14***, 3977-3986 (2008).
18. Mizoshita, N., Kutsuna, T., Kato, T., and Hanabusa, K. Smectic liquid-crystalline physical gels. Anisotropic self-aggregation of hydrogen-bonded molecules in layered structures, *Chem. Commun.* 781-782 (1999).
19. Karsai, Á., Murvai, Ü., Soós, K., Penke, B., and Kellermayer, M. S. Oriented epitaxial growth of amyloid fibrils of the N27C mutant β25–35 peptide, *Eu. Biophy. J. **37***, 1133-1137 (2008).
20. Li, Z., Jing, C., Chen, J., Yuan, S., Cao, S., and Zhang, J. Observation of exchange bias in the martensitic state of Ni 50 Mn 36 Sn 14 Heusler alloy, *Appl. Phy. Let.**91***, 112505 (2007).
21. Chivers, P. R., and Smith, D. K. Shaping and structuring supramolecular gels, *Nature Rev. Mater. **4***, 463-478 (2019).
22. Ding, R., Yu, X., Wang, P., Zhang, J., Zhou, Y., Cao, X., Tang, H., Ayres, N., and Zhang, P. Hybrid photosensitizer based on amphiphilic block copolymer stabilized silver nanoparticles for highly efficient photodynamic inactivation of bacteria, *RSC Adv. **6***, 20392-20398 (2016).
23. Krall, A. H., and Weitz, D. A. Internal Dynamics and Elasticity of Fractal Colloidal Gels, *Phys. Rev. Let.**80***, 778-781 (1998).
24. Li, L., Wang, Y., Pan, L., Shi, Y., Cheng, W., Shi, Y., and Yu, G. A nanostructured conductive hydrogels-based biosensor platform for human metabolite detection, *Nano Let.**15***, 1146-1151 (2015).
25. Pan, L., Yu, G., Zhai, D., Lee, H. R., Zhao, W., Liu, N., Wang, H., Tee, B. C.-K., Shi, Y., and Cui, Y. Hierarchical nanostructured conducting polymer hydrogel with high electrochemical activity, *Proce. Nation. Aca. Sci. **109***, 9287-9292 (2012).
26. Zhai, D., Liu, B., Shi, Y., Pan, L., Wang, Y., Li, W., Zhang, R., and Yu, G. Highly sensitive glucose sensor based on Pt nanoparticle/polyaniline hydrogel heterostructures, *ACS nano**7***, 3540-3546 (2013).
27. Cornwell, D. J., Okesola, B. O., and Smith, D. K. Multidomain hybrid hydrogels: spatially resolved photopatterned synthetic nanomaterials combining polymer and low molecular weight gelators, *Angew. Chemie**126***, 12669-12673 (2014).
28. de Jong, J. J., Hania, P. R., Pugžlys, A., Lucas, L. N., de Loos, M., Kellogg, R. M., Feringa, B. L., Duppen, K., and van Esch, J. H. Light driven dynamic pattern formation, *Angew. Chemie Interna. Ed. **44***, 2373-2376 (2005).
29. Draper, E. R., Eden, E. G., McDonald, T. O., and Adams, D. J. Spatially resolved multicomponent gels, *Nature Chem.**7***, 848 (2015).
30. Eastoe, J., Sánchez-Dominguez, M., Wyatt, P., and Heenan, R. K. A photo-responsive organogel, *Chem. Commun.*, 2608-2609 (2004).
31. Nolan, M. C., Caparrós, A. M. F., Dietrich, B., Barrow, M., Cross, E. R., Bleuel, M., King, S. M., and Adams, D. J. Optimising low molecular weight hydrogels for automated 3D printing, *Soft Mat.**13***, 8426-8432 (2017).

32. Wei, Q., Xu, M., Liao, C., Wu, Q., Liu, M., Zhang, Y., Wu, C., Cheng, L., and Wang, Q. Printable hybrid hydrogel by dual enzymatic polymerization with superactivity, *Chem. Sci.**7***, 2748-2752 (2016).
33. Raeburn, J., Alston, B., Kroeger, J., McDonald, T. O., Howse, J. R., Cameron, P. J., and Adams, D. J. Electrochemically-triggered spatially and temporally resolved multi-component gels, *Materials Horizons**1***, 241-246 (2014).
34. Inostroza-Brito, K. E., Collin, E., Siton-Mendelson, O., Smith, K. H., Monge-Marcet, A., Ferreira, D. S., Rodríguez, R. P., Alonso, M., Rodríguez-Cabello, J. C., and Reis, R. L. Co-assembly, spatiotemporal control and morphogenesis of a hybrid protein-peptide system, *Nature Chem.**7***, 897 (2015).
35. Olive, A. G., Abdullah, N. H., Ziemecka, I., Mendes, E., Eelkema, R., and Van Esch, J. H. Spatial and directional control over self-assembly using catalytic micropatterned surfaces, *Angew. Chemie **53***, 4132-4136 (2014).
36. Rodon Fores, J., Martinez Mendez, M. L., Mao, X., Wagner, D., Schmutz, M., Rabineau, M., Lavalle, P., Schaaf, P., Boulmedais, F., and Jierry, L. Localized supramolecular peptide self-assembly directed by enzyme-induced proton gradients, *Angew. Chemie**129***, 16200-16204 (2017).
37. Hu, B., Owh, C., Chee, P. L., Leow, W. R., Liu, X., Wu, Y.-L., Guo, P., Loh, X. J., and Chen, X. Supramolecular hydrogels for antimicrobial therapy, *Chem. Soc. Rev. **47***, 6917-6929 (2018).
38. Okesola, B. O., and Smith, D. K. Applying low-molecular weight supramolecular gelators in an environmental setting-self-assembled gels as smart materials for pollutant removal, *Chem. Soc. Rev. **45***, 4226-4251 (2016).
39. Weiss, R. G., Blair, D., Toro-Vazquez, J. F., Liu, X.-Y., Escuder, B., Rogers, M. A., Ajayaghosh, A., Guenet, J.-M., Smith, D., and Steed, J. *Mol. Gels: Str. Dynam. Royal Soc. Chem*. (2018).
40. Bordes, R., Tropsch, J., and Holmberg, K. Counterion specificity of surfactants based on dicarboxylic amino acids, *J. Colloid and Interface Sci. **338***, 529-536 (2009).
41. Maiti, K., Bhattacharya, S. C., Moulik, S. P., and Panda, A. K. Physicochemical studies on ion-pair amphiphiles: Solution and interfacial behaviour of systems derived from sodium dodecylsulfate and n-alkyltrimethylammonium bromide homologues, *J. Chem. Sci.**122***, 867-879 (2010).
42. Li, J.-L., and Liu, X.-Y. (2009) Microengineering of soft functional materials by controlling the fiber network formation, *J. Phys. Chem. B**113***, 15467-15472.
43. Li, S., Funahashi, R., Matsubara, I., Ueno, K., Sodeoka, S., and Yamada, H. Synthesis and Thermoelectric Properties of the New Oxide Materials $Ca_{3-x}Bi_xCo_4O_9+\delta$ ($0.0< x< 0.75$), *Chem. Mater.**12***, 2424-2427 (2000).
44. Herwig, P., Kayser, C. W., Müllen, K., and Spiess, H. W. Columnar mesophases of alkylated hexa-peri-hexabenzocoronenes with remarkably large phase widths, *Adv. Mater.**8***, 510-513 (1996).
45. Barai, M., Mandal, M. K., Karak, A., Bordes, R., Patra, A., Dalai, S., and Panda, A. K. Interfacial and aggregation behavior of dicarboxylic amino acid based surfactants in combination with a cationic surfactant, *Langmuir* (2019).

46. Maréchal, J.-P., Matsumura, K., Conlan, S., and Hellio, C. Competence and discrimination during cyprid settlement in Amphibalanus amphitrite, *Intern. Biodeterior. Biodegrad.**72***, 59-66 (2012).
47. Van der Kooij, F. M., and Lekkerkerker, H. N. Formation of nematic liquid crystals in suspensions of hard colloidal platelets, *J. Phys. Chem. B**102***, 7829-7832 (1998).
48. Fan Shao, R., Willis, P. C., and Clark, N. A. The field induced stripe texture in surface stabilized ferroelectric liquid crystal cells, *Ferroelectrics**121***, 127-136 (1991).
49. Kokini, J. L., Kadane, J. B., and Cussler, E. L. Liquid texture perceived in the mouth1, *J. Texture Stu. **8***, 195-218 (1977).
50. Baral, A., Roy, S., Dehsorkhi, A., Hamley, I. W., Mohapatra, S., Ghosh, S., and Banerjee, A. Assembly of an injectable noncytotoxic peptide-based hydrogelator for sustained release of drugs, *Langmuir**30***, 929-936 (2014).
51. Kalafatovic, D., Nobis, M., Javid, N., Frederix, P. W., Anderson, K. I., Saunders, B. R., and Ulijn, R. V. MMP-9 triggered micelle-to-fibre transitions for slow release of doxorubicin, *Biomaterials Sci.**3***, 246-249 (2015).
52. Criado-Gonzalez, M., Rodon Fores, J., Wagner, D., Schröder, A. P., Carvalho, A., Schmutz, M., Harth, E., Schaaf, P., Jierry, L., and Boulmedais, F. Enzyme-assisted self-assembly within a hydrogel induced by peptide diffusion, *Chem. Commun.**55***, 1156-1159 (2019).
53. Bag, B. G., Hasan, S. N., Pongpamorn, P., and Thasana, N. First hierarchical self-assembly of a seco-triterpenoid α-onocerin yielding supramolecular architectures, *Chem. Select**2***, 6650-6657 (2017).
54. Piras, C., Slavik, P., and Smith, D. K. Self-assembling supramolecular hybrid hydrogel beads, *Angew. Chemie Intern. Ed.*
55. Bhattacharya, S., and Acharya, S. G. Pronounced hydrogel formation by the self-assembled aggregates of N-alkyl disaccharide amphiphiles, *Chem. Mater.**11***, 3504-3511 (1999).
56. Datta, S., and Bhattacharya, S. Multifarious facets of sugar-derived molecular gels: molecular features, mechanisms of self-assembly and emerging applications, *Chem. Soc. Rev.**44***, 5596-5637 (2015).
57. Uva, M., and Atrei, A. Surface morphology at the microscopic scale, swelling/deswelling, and the magnetic properties of pnipam/CMC and pnipam/cmc/Fe_3O_4 hydrogels, *Gels**2***, 30 (2016).
58. Mukherjee, A., Dateer, R. B., Chaudhuri, R., Bhunia, S., Karad, S. N., and Liu, R.-S. Gold-catalyzed 1, 2-difunctionalizations of aminoalkynes using only N-and O-containing oxidants, *J. Am. Chem. Soc.**133***, 15372-15375 (2011).
59. Sui, L., Wang, F., and Li, B. Adult-onset hypothyroidism impairs paired-pulse facilitation and long-term potentiation of the rat dorsal hippocampo-medial prefrontal cortex pathway in vivo, *Brain Res.1096*, 53-60 (2006).
60. Varughese, P., Saban, K., George, J., Paul, I., and Varghese, G. Crystallization and structural properties of calcium malonate hydrate, *J. Mater. Sci. **39***, 6325-6331 (2004).

61. Xia, Y., Tse, C., and Lau, F. C.-M. Performance of differential chaos-shift-keying digital communication systems over a multipath fading channel with delay spread, *IEEE Transactions on Circuits and Systems II: Express Briefs* ***51***, 680-684 (2004).
62. Weiss, I. M., Muth, C., Drumm, R., and Kirchner, H. O. Thermal decomposition of the amino acids glycine, cysteine, aspartic acid, asparagine, glutamic acid, glutamine, arginine and histidine, *BMC biophysics11*, 2 (2018).
63. Nahak, P., Karmakar, G., Chettri, P., Roy, B., Guha, P., Besra, S. E., Soren, A., Bykov, A. G., Akentiev, A. V., and Noskov, B. A. Influence of lipid core material on physicochemical characteristics of an ursolic acid-loaded nanostructured lipid carrier: An attempt to enhance anticancer activity, *Langmuir* ***32***, 9816-9825 (2016).
64. Jemal, A., Siegel, R., Ward, E., Murray, T., Xu, J., and Thun, M. J. Cancer statistics, 2007, *CA: A Cancer J. Clinic.* ***57***, 43-66 (2007).
65. Sun, M.-L., Zhao, F., Shi, M., Zhang, X.-Y., Zhou, B.-C., Zhang, Y.-Z., and Chen, X.-L. Characterization and Biotechnological Potential Analysis of a New Exopolysaccharide from the Arctic Marine Bacterium Polaribacter sp. SM1127, *Sci. Rep. 5*, 18435 (2015).
66. Bordes, R., and Holmberg, K. Physical chemical characteristics of dicarboxylic amino acid-based surfactants, *Colloids and Surf. A:* ***391***, 32-41 (2011).
67. Kaler, E. W., Herrington, K. L., Murthy, A. K., and Zasadzinski, J. A. Phase behavior and structures of mixtures of anionic and cationic surfactants, *J. Phys. Chem.* ***96***, 6698-6707 (1992).
68. Choffat, F., Käser, S., Wolfer, P., Schmid, D., Mezzenga, R., Smith, P., and Caseri, W. Synthesis and characterization of linear poly (dialkylstannane) s, *Macromolecules* ***40***, 7878-7889 (2007).
69. Sastry, N. V., and Singh, D. K. Surfactant and gelation properties of acetylsalicylate based room temperature ionic liquid in aqueous media, *Langmuir* ***32***, 10000-10016 (2016).
70. Preston, K. L., Bigelow, G. E., Bickel, W. K., and Liebson, I. A. Drug discrimination in human postaddicts: agonist-antagonist opioids, *J. Pharmacol. Experi. Therap.* ***250***, 184-196 (1989).
71. Weichert, A., and Hoffmann, H. M. R. Synthesis and reactions of. alpha.-methylene-. beta.-keto sulfones, *J. Org. Chem.* ***56***, 4098-4112 (1991).
72. Agbaje, T., Mondal, S., Makukula, Z., Motsa, S., and Sibanda, P. A new numerical approach to MHD stagnation point flow and heat transfer towards a stretching sheet, *Ain Shams Engin. J.* ***9***, 233-243 (2018).
73. Sufian, A., and Russell, A. R. Microstructural pore changes and energy dissipation in Gosford sandstone during pre-failure loading using X-ray CT, *Intern. J. Rock Mech. Min. Sci.* ***57***, 119-131 (2013).

Figures

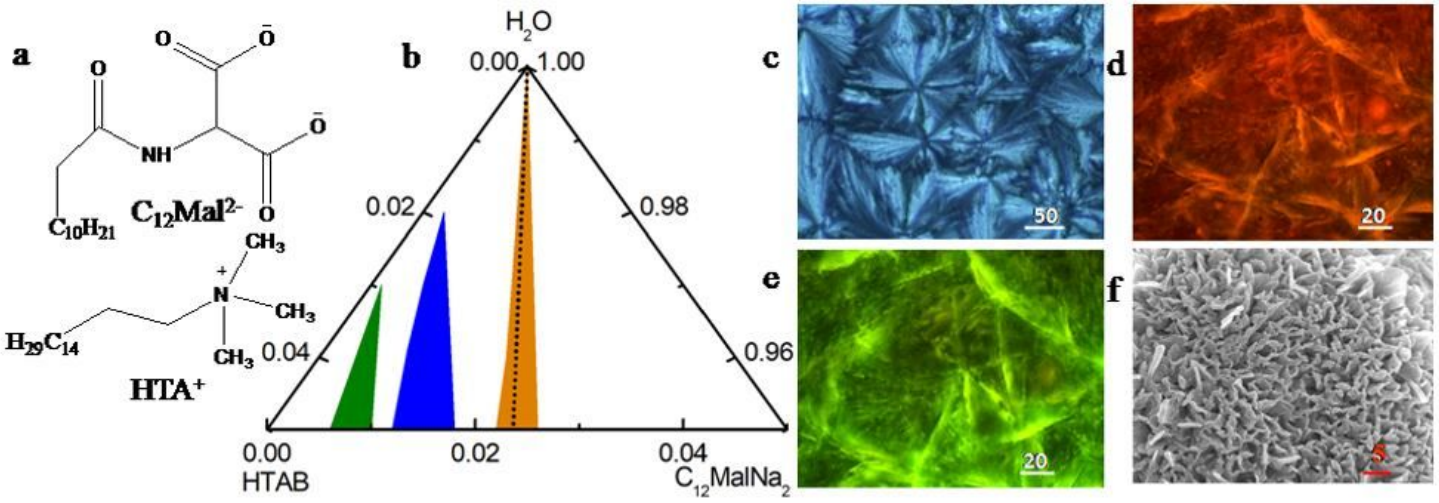

Figure 1

a, Chemical structure of C12MalNa2 and HTAB; b, truncated phase diagram of C12MalNa2 + HTAB + water mixed system. Phases: olive, gel; blue, viscous; orange, precipitate; and clear region indicate micelle. Dotted line in panel b corresponds to equimolar region. Panel c, POM image; d and e, FM images of rhodamine-B and fluorescein stained 5 wt% C12MalNa2 + HTAB (40:60, w/w) gel. Panel f, FE-SEM image of same gel. Scale bars (in μm) are mentioned in the microscopic images.

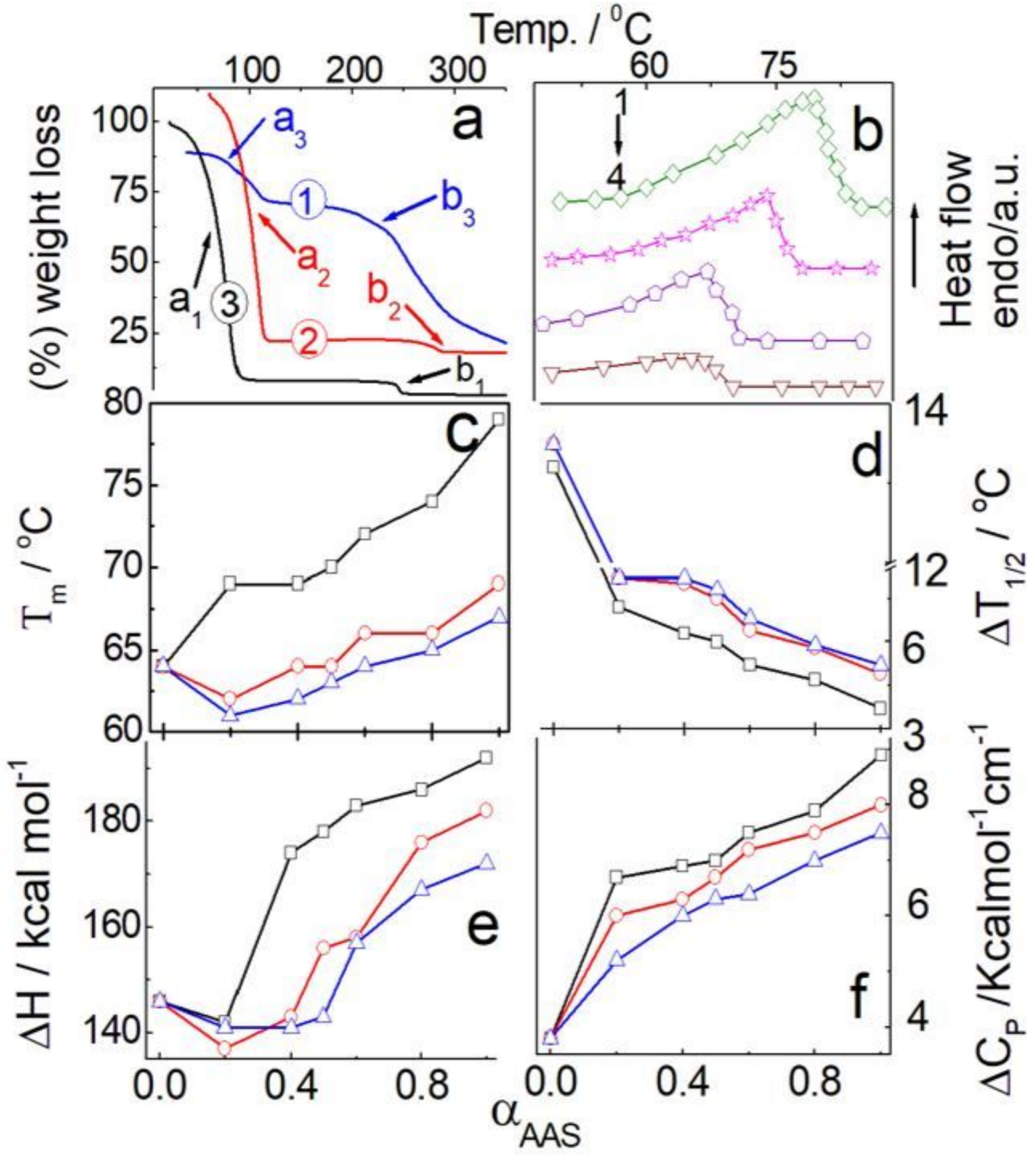

Figure 2

(a), TGA thermogram of AAS+ HTAB (100mM, 40/60, M/M) gel. Systems: 1; C12GluNa2 + HTAB, 2, C12AspNa2 + HTAB and 3, C12MalNa2 + HTAB. a1, b1, a2, b2, a3, and b3 represent different phase transitions. (b), DSC thermograms of C12MalNa2 + HTAB mixture at different mole% of C12MalNa2: 1; 80, 2; 60, 3; 40, and 4; 0. Variations of (c), Tm; (d), ΔT1/2; (e), ΔH and (f), ΔCp with the mole fraction of AASs (αAAS). Systems: The line colors in panel (c), (d), (e) and (f) are representing similar surfactant mixture composition as in panel (a).

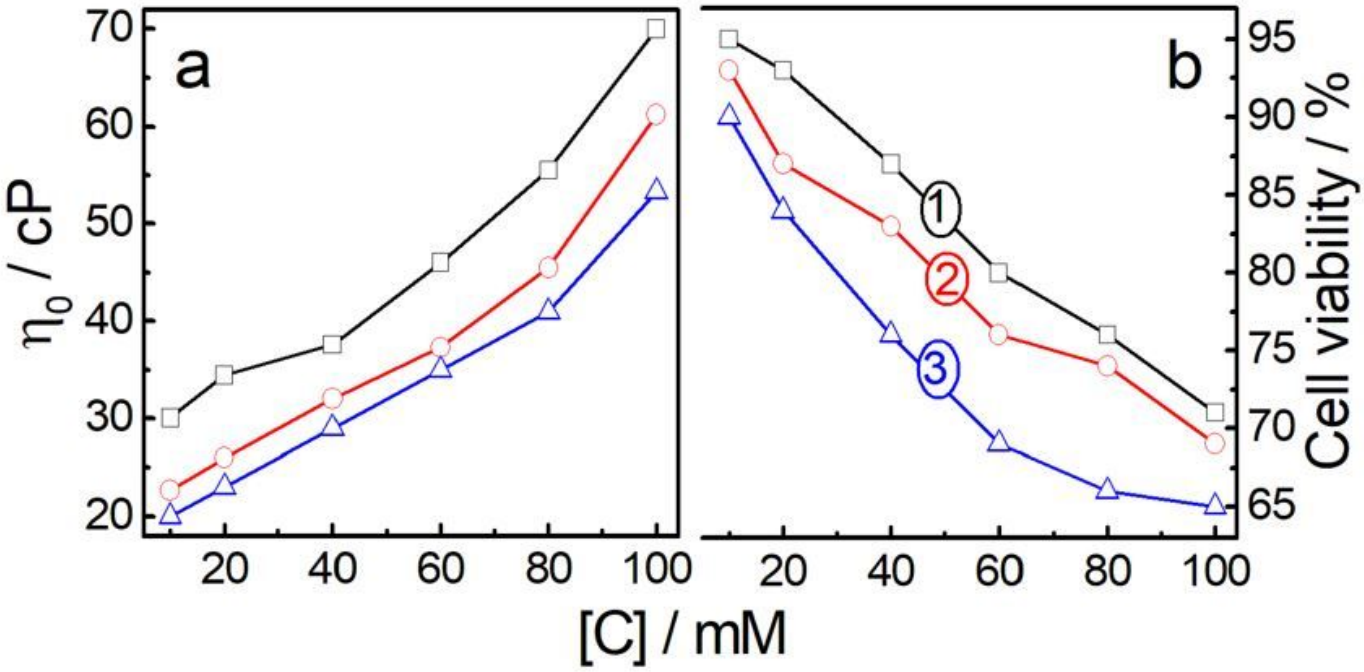

Figure 3

Variation of a, zero share viscosity and b, human blood lymphocyte cell viability with AASs + HTAB (2/3, M/M) mixed surfactant concentration [C]. Systems: 1; C12GluNa2 + HTAB, 2, C12AspNa2 + HTAB and 3, C12MalNa2 + HTAB.

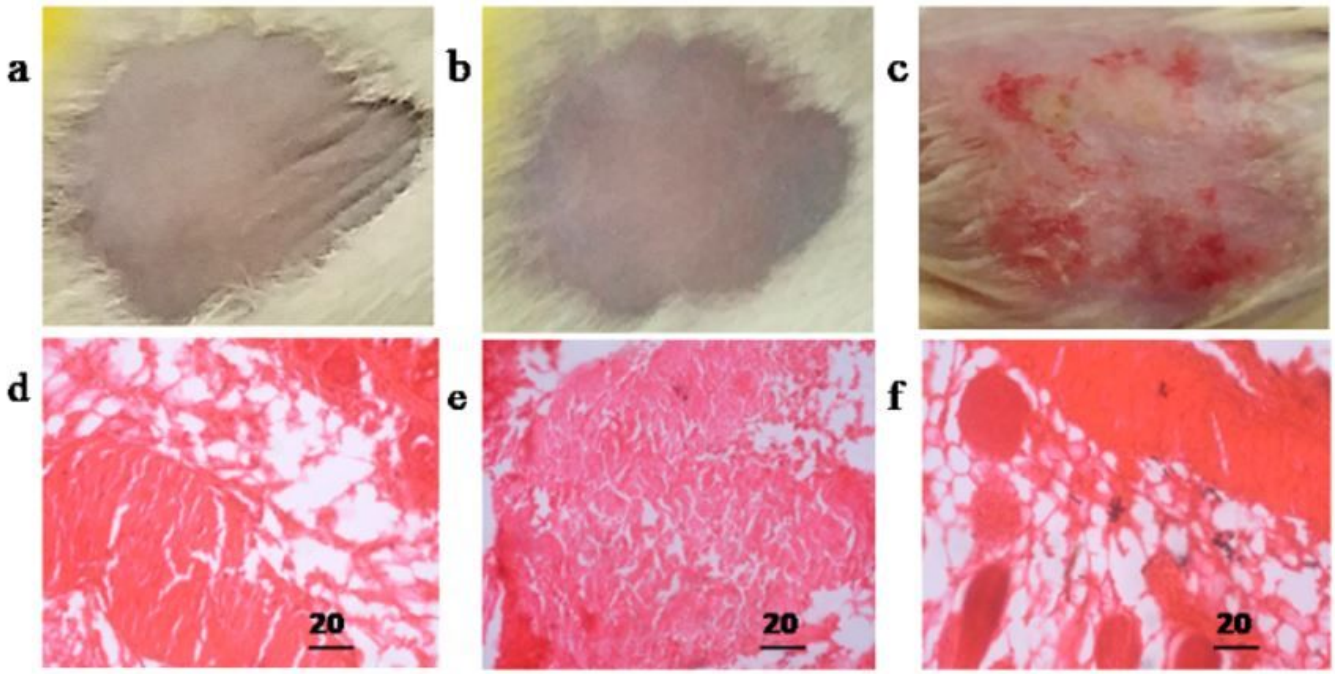

Figure 4

Skin irritation (a, b, c) and histological (d, e, f) tests on the dorsal area of trunk region of Swiss albino mice. a and d, negative control (mice were treated with sterile distilled water); c and f, positive control (mice were treated with 5% phenol-water; b and e, mice were treated with C12MalNa2 + HTAB gel (100 mM, 60/40, M/M). Scale bar for the microscopic images: 20 μm.

Supplementary Files

This is a list of supplementary files associated with this preprint. Click to download.

- SupplementarysectionBarai.docx